

Original Article

Establishment and validation of a T12-L2 3D finite element model for thoracolumbar segments

Hui Lu^{1,2,3*}, Qichuan Zhang^{4*}, Fan Ding^{1,2}, Qimei Wu⁵, Rong Liu^{1,2,3}

¹School of Medicine, Wuhan University of Science and Technology, Wuhan 430065, Hubei, China; ²Department of Orthopedics, Puren Hospital Affiliated to Wuhan University of Science and Technology, Wuhan 430081, Hubei, China; ³Institute of Medical Innovation and Transformation, Puren Hospital Affiliated to Wuhan University of Science and Technology, Wuhan 430081, Hubei, China; ⁴Department of Radiology, The Second Affiliated Hospital of Army Military Medical University, Chongqing 400037, China; ⁵Wuhan Liu Sanwu Hospital of Traditional Chinese Medicine, Xinzhou District, Wuhan 430081, Hubei, China. *Equal contributors.

Received August 31, 2021; Accepted January 24, 2022; Epub March 15, 2022; Published March 30, 2022

Abstract: Objective: To establish and verify the validity of a three-dimensional finite element model of the thoracolumbar segments T12-L2; the stress distribution of the model was analyzed, providing a theoretical basis for finite element analysis of thoracolumbar segment fracture as well as a surgical model. Methods: A healthy female volunteer with no history of lumbar spine injury was selected to obtain CT scan data of the T12-L2 vertebral bodies. Mimics 3D reconstruction software was used to generate the T12-L2 3D model, and surface mesh and body mesh were generated by smoothing treatment and mesh division. The normal finite element model of the T12-L2 vertebral bodies and the finite element model of osteoporosis were established with Ansys finite element software. Under a loading force of 500 N vertically downward and a load of 7.5 N • m bending moment, seven operating conditions were simulated to analyze the displacement and stress distribution of each vertebral body and intervertebral disc, and to verify the effectiveness of the model. Results: There were 31,901 nodes and 64,244 elements in the thoracolumbar T12-L2 three-dimensional finite element model. These results were similar to the conclusions found in a review of the domestic and global literature, and the finite element model was validated. Conclusions: The results of this experiment can provide a practical reference for clinical work and help to establish a three-dimensional finite element model of the thoracolumbar junction.

Keywords: Finite element analysis, thoracolumbar segment, biomechanics, spine

Introduction

Vertebral compression fractures usually occur at the thoracolumbar junction (T11-L2 level), which can lead to kyphosis at the site of spinal fracture, and in severe cases it affects function and quality of life [1]. The traditional method of measuring spinal biomechanics with cadaver specimens is useful for understanding displacement of certain structures, but the stress changes to the internal structures and fixators are difficult to measure. Animal experiments can be used to evaluate the stability of bone graft fusion segments, but the results do not completely apply to humans.

In recent years, quantitative CT (QCT) examination of lumbar vertebra specimens and finite

element models have been used to simulate and calculate vertebral bone strength. Compared with experimental results from biomechanical testing of vertebral bodies, the PEA model derived from QCT images may improve the predictive ability for vertebral strength [2, 3]. Belytschko et al. first proposed the application of the finite element method using computer technology to biomechanical study of the spine [4]. Further studies have applied the finite element method to study spine biomechanics, achieving successful results [5, 6].

Chen et al. performed a biomechanical study of interbody fusion through a foraminal approach with unilateral and bilateral pedicle screw fixation using a three-dimensional finite element method [7]. Goel and Gilbertson used the finite

Biomechanical analysis of the spine

Table 1. Material properties of the osteoporotic T12-L2 finite element model

Material	Elastic modulus, E (MPa)	Poisson ratio, μ	Stiffness Coefficient	Status
Cortical bone	8040 (67% normal)	0.3	-	Osteoporotic
Cancellous bone	34 (34% normal)	0.2	-	Osteoporotic
Bony endplate	670 (67% normal)	0.4	-	Osteoporotic
Posterior structure	2345 (67% normal)	0.25	-	Osteoporotic
Annulus fibers	455	0.3	-	Normal
Nucleus pulposus	0.4	0.499	-	Normal
Facet cartilage	10	0.4	-	Normal
Anterior longitudinal	20	0.3	33.0	Normal
Posterior longitudinal	70	0.3	20.4	Normal
Interspinous	28	0.3	11.5	Normal
Supraspinous	28	0.8	23.7	Normal
Ligamentum flavum	50	0.3	27.2	Normal
Intertransverse	50	0.3	15.0	Normal

element method to study the biomechanics of the thoracolumbar spine [8]. Although the usefulness of spinal finite element analysis has been demonstrated in many studies [9-13], accurate three-dimensional finite element models of the thoracolumbar segment are rarely reported.

In the current experiment, the thoracolumbar T12-L2 three-dimensional finite element model was used to simulate seven operating conditions (axial direction, antelexion, rear protraction, left side and right side bending, and left and right rotation) under a loading force of 500 N vertically downward and a load of 7.5 N•m bending moment. The stress distribution for each vertebral body and intervertebral disc was analyzed, and the validity of the model was verified. The results provide a theoretical basis for finite element analysis of thoracolumbar fractures and a surgical model.

Materials and methods

Design

Finite element analysis experiment.

Data collection

A healthy 65-year-old female volunteer with no significant abnormalities in vertebral body morphology was scanned, and T12-L2 CT data were obtained. The volunteer was screened for cardiovascular and cerebrovascular diseases, severe liver or renal impairments, and mental

illness. The patient and her family agreed to participate in the study and signed the informed consent, and the experimental protocol was approved by our hospital ethics committee. The lumbar vertebral bodies were scanned with Siemens 64-slice spiral CT at 140 kV, 200 mA, and 0.625 mm thickness. CT data were extracted in 512×512 pixel DICOM format.

Methods

Establishment of the T12-L2 three-dimensional finite

element model for normal and osteoporosis thoracolumbar segments: The CT data of the volunteer was imported into the Mimics 20.0 software. According to the gray value of each tissue structure, the threshold was divided, and models of different parts of the lumbar spine were established. The regions of interest were segmented by image cutting tools, and the models were preliminarily processed by filling, wrapping, smoothing, and other tools. The resulting geometric model of T12-L2 vertebral body and intervertebral disc was established and exported in STL format. The three-dimensional model of the lumbar spine was imported into 3-matic 12.0 in STL format, and the surface of the lumbar spine was smoothed and measured through mesh diagnosis, treatment of poor mesh, surface parameter fitting, and other operations. The vertebral body was simulated as the inner core of the spongy bone surrounded by cortical bone, with the disc covered with cartilage endplates [14]. Intervertebral discs are composed of an outer annulus fibrosus and an inner nucleus pulposus, and the cross-sectional area of the nucleus pulposus accounts for 43% of the intervertebral disc cross-sectional area [15]. The interaction between joints was simulated by nonlinear surface-bound contact. Ligaments were simulated by a 2-node nonlinear spring element. After ensuring that all surface meshes were qualified, the body meshes of the lumbar spine model were generated. Finally, the entire model was generated.

Biomechanical analysis of the spine

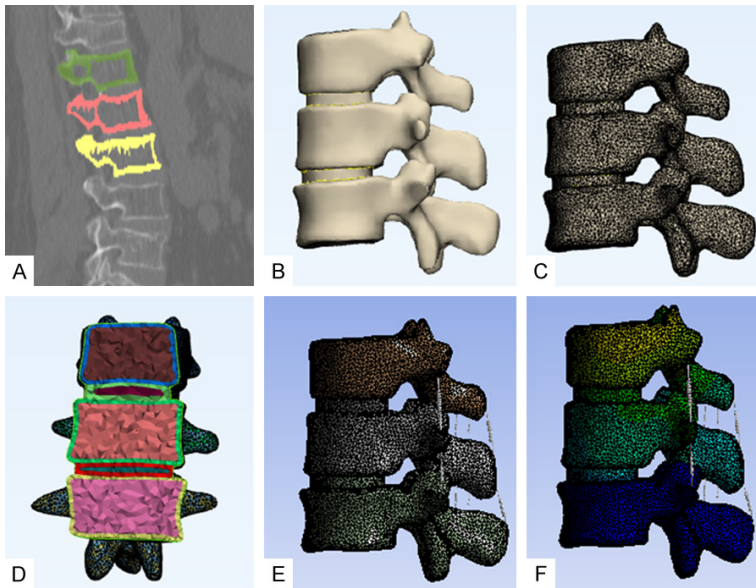


Figure 1. T12-L2 Three-dimensional finite element model of thoracolumbar segment. A. Threshold extraction; B. Smooth processing; C. Meshing; D. Solid model; E. Spring simulation ligament; F. Finite element model.

Table 2. Range of motion of finite element model of T12-L2 and comparison with previous research result (°)

Operating Condition	The Present Research	[21]	[23]	[24]	The Present OP Model
Ante-flexion	6.8±2.15	7.0	7.8	7.9	6.9
Rear Protraction	5.0±1.34	4.5	5.5	6.8	4.8
Left Side Bending	5.5±1.75	7.5	8.1	7.3	5.7
Right Side Bending	5.3±1.44	-	-	8.0	5.5
Left Rotation	2.2±1.42	3.1	2.6	2.8	2.6
Right Rotation	2.5±1.36	-	-	3.3	2.7
Axial Direction	-	-	-	-	-

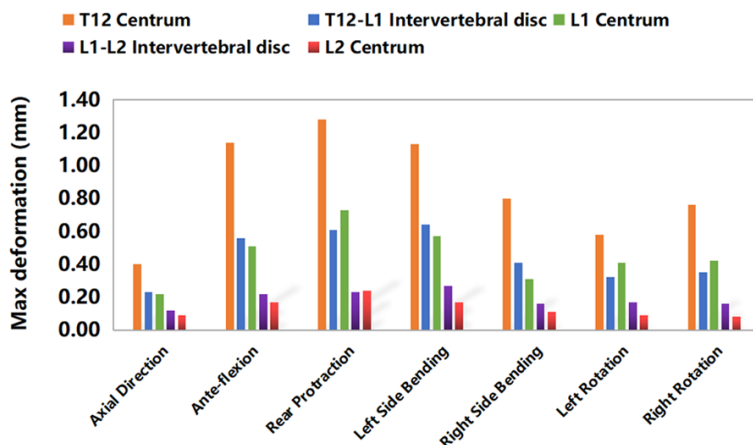


Figure 2. Deformation results of T12-L2 finite element model of thoracolumbar section under seven working conditions.

The model was imported into Mimics 20.0, and the elastic modulus, Poisson's ratio and other material coefficients and characteristic values of the materials in each area were input into the model to set the material properties. In this study, in order to streamline the calculation process, the material properties were simplified in the mechanical analysis. Only the mechanical properties of the bone structure within the elastic range were considered, and the isotropic, uniform, and continuous elastic material model was used to characterize the bone structure. According to previous reports [16-20] we characterized the specific material parameters (Table 1).

Validation of the model: After completing the assignment of the material attributes, the lower endplate of the L2 vertebral body was set as the fixed surface, and the load was allocated from the upper endplate of the T12 vertebral body according to the theory of the three columns of the spine, in which 85% of the load was carried by the anterior midcolumn and the remaining 15% of the load was carried by the elements behind the vertebrae [21, 22]. All models were subjected to a vertical downward load of 500 N and a torque of 7.5 N•m to simulate the physiological activity of the lumbar spine under the seven rotational directions (axial direction, ante-flexion, rear protraction, left side and right side bending, and left and right rotation).

Observational index

The deformation and von-Mises stress distribution for each

Biomechanical analysis of the spine

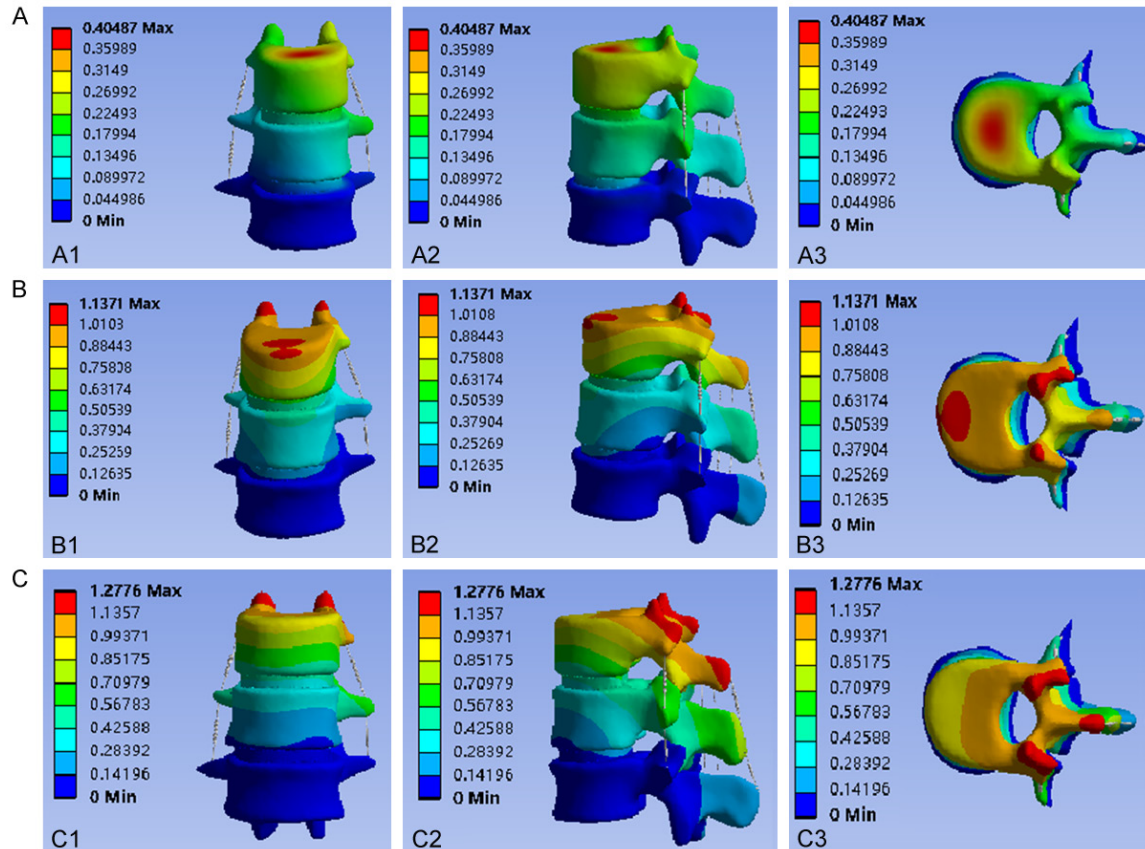


Figure 3. Three-view results of deformation distribution of T12-L2 finite element model in thoracic and lumbar segments in Axial Direction, Ante-flexion and Rear Protraction. (A1) Axial Direction-front view, (A2) Axial Direction-side view, (A3) Axial Direction-top view; (B1) Ante-flexion-front view, (B2) Ante-flexion-side view, (B3) Ante-flexion-top view; (C1) Rear Protraction-front view, (C2) Rear Protraction-side view, (C3) Rear Protraction-top view.

vertebral body and intervertebral disc were observed in the thoracolumbar T12-L2 finite element model under seven working conditions: axial direction, ante-flexion, rear protraction, left side and right side bending, and left and right rotation.

Results

T12-L2 three-dimensional finite element model structure of thoracolumbar segment

A 3D finite element model of the thoracolumbar T12-L2 segment was established. The model simulated the three-dimensional structures of cortical and spongy bone, annulus fibrosus and nucleus pulposus, facet joint, pedicle, lamina, spinous and transverse processes, and the intertransverse process, interspinous, and supraspinous ligaments. After non-popular assembly node sharing and standardized grid processing, the complete final model had 31,901 nodes and 64,244 cells (**Figure 1**).

Validation results of the model

In this study, the loading analysis of normal and osteoporotic lumbar finite element model under seven working directions (axial direction, ante-flexion, rear protraction, left side and right side bending, and left and right rotation) was conducted, and the range of motion (ROM) of the joint under various working conditions was measured. The results obtained were highly similar to published findings in the domestic and global literature [21, 23, 24] (**Table 2**), and the finite element model verifies the validity.

Deformation and von-mises stress distribution of the T12-L2 finite element model in the thoracolumbar section under seven working conditions

We obtained deformation results of the T12-L2 finite element model in the thoracolumbar section under seven working conditions (**Figure 2**). The degree of deformation was in the order of

Biomechanical analysis of the spine

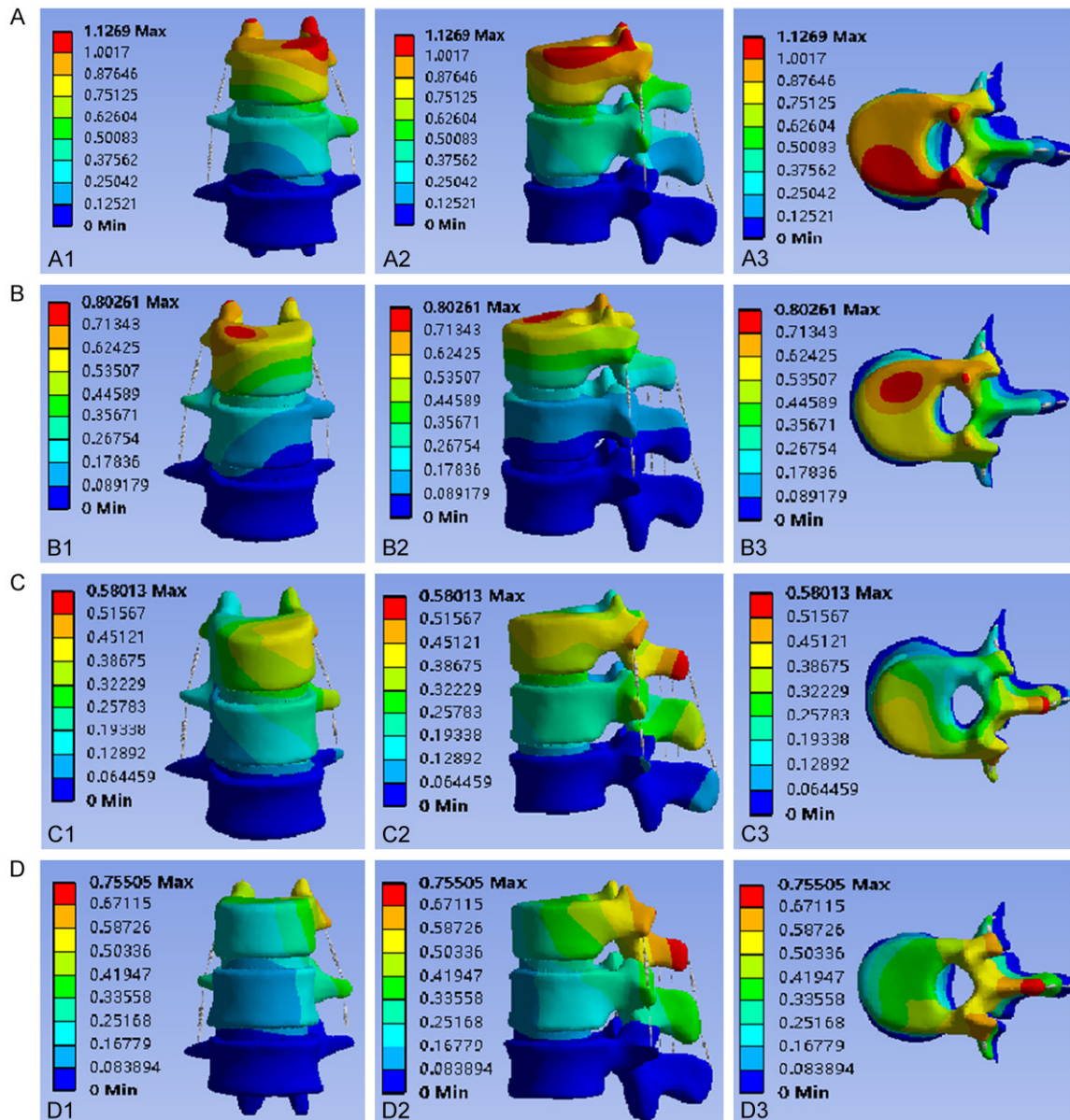


Figure 4. Results of deformation distribution of the T12-L2 finite element model in the thoracic and lumbar segments in three views under the states of Left Side Bending, Right Side Bending, Left Rotation and Right rotation. (A1) Left Side Bending-front view, (A2) Left Side Bending-side view, (A3) Left Side Bending-top view; (B1) Right Side Bending-front view, (B2) Right Side Bending -side view, (B3) Right Side Bending-top view; (C1) Left Rotation-front view, (C2) Left Rotation-side view, (C3) Left Rotation-top view; (D1) Right rotation-front view, (D2) Right rotation-side view, (D3) Right rotation-top view.

anteflexion/rear protraction > side bending > rotation > axial direction. Under each condition, the degree of deformation gradually decreased from the upper endplate of T12 to the lower endplate of L2. We obtained three-view results of the deformation distribution of the T12-L2 finite element model in the thoracic and lumbar segments in axial, bending, and stretching states (Figure 3) and in the states of left

and right bending, and left and right rotation (Figure 4).

We measured the stress distribution of the T12-L2 finite element model in the thoracolumbar section under seven working conditions (Figure 5). The stress of the disc under various working conditions was significantly less than that of the vertebral body, and the stress distri-

Biomechanical analysis of the spine

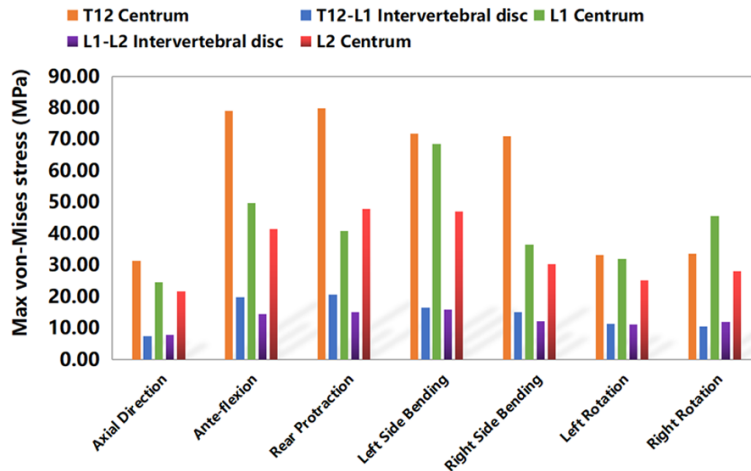


Figure 5. von-Mises stress distribution results of T12-L2 finite element model in thoracic and lumbar section under seven working conditions.

bution was $T12 > L1 > L2$. The stress on the vertebral body under flexion, extension, and lateral bending conditions was significantly higher than under the rotation and axial conditions. We obtained three-view results of stress distribution of the T12-L2 finite element model in the thoracic and lumbar segments in axial, bending, and stretching states (Figure 6) and with the conditions of left and right bending, and left and right rotation (Figure 7).

Discussion

Previous applications of finite elements in the spine

Geometry, material properties, and appropriate loads are the key elements in validation of the finite element model of the spine [25, 26]. With advances in technology, finite element models are now used in various studies of spinal dynamics, kinematics, and stress and strain within the vertebrae and intervertebral discs [27-31]. Recent improvements to software technology and computing capability have enabled reconstruction of three-dimensional models of irregular spinal bone structure using CT technology [32, 33]. The current study is also based on the use of CT data for 3D reconstruction.

In a previous study, Giambini et al. applied the finite element method to predict vertebral fracture characteristics [34]. From three cadaver specimens, the L3 vertebral bodies were

excised. The vertebrae were scanned with CT to establish the computational model and then subjected to mechanical compression tests to measure failure loads and stiffness, and to observe fracture locations. A vertebra was used to calibrate the material properties based on the experimental results and CT gray values. The other two samples were used to evaluate model predictions. The finite element model of the calibrated sample had an error of 2% in stiffness and of 4% in failure load. The predicted failure loads for the other

two vertebrae were greater, with stiffness differences of 129% and 40% compared to the measured values. The predicted fracture pattern was in agreement with the observed experimental cracks. Thus, the finite element method can be used to predict vertebral fracture characteristics.

Xu et al. compared the biomechanical differences between posterior lumbar interbody fusion (PLIF) and transforaminal lumbar interbody fusion (TLIF) by using the finite element method [5]. Three L3-L5 lumbar segment finite element models (complete, PLIF, and TLIF models) were established. To analyze the biomechanical properties of these models, a torque of 7.5 N•m was applied to the upper surface of the L3 vertebral body with a compressive preload of 400 N. Compared with the full model, the PLIF and TLIF models had a reduced range of motion at the L4-L5 level under all loading conditions, although when PLIF and TLIF were less than 1 degree, there was no significant difference in the range of motion. That study concluded that TLIF surgery could reduce the risks and limitations associated with PLIF and provide a suitable alternative to PLIF surgery.

Baroud et al. quantified and compared the stiffness and load response of adjacent enhanced discs before and after enhancement by establishing a finite element model of the lumbar motor segment (L4-L5) [17]. The results showed that the cement under the endplate

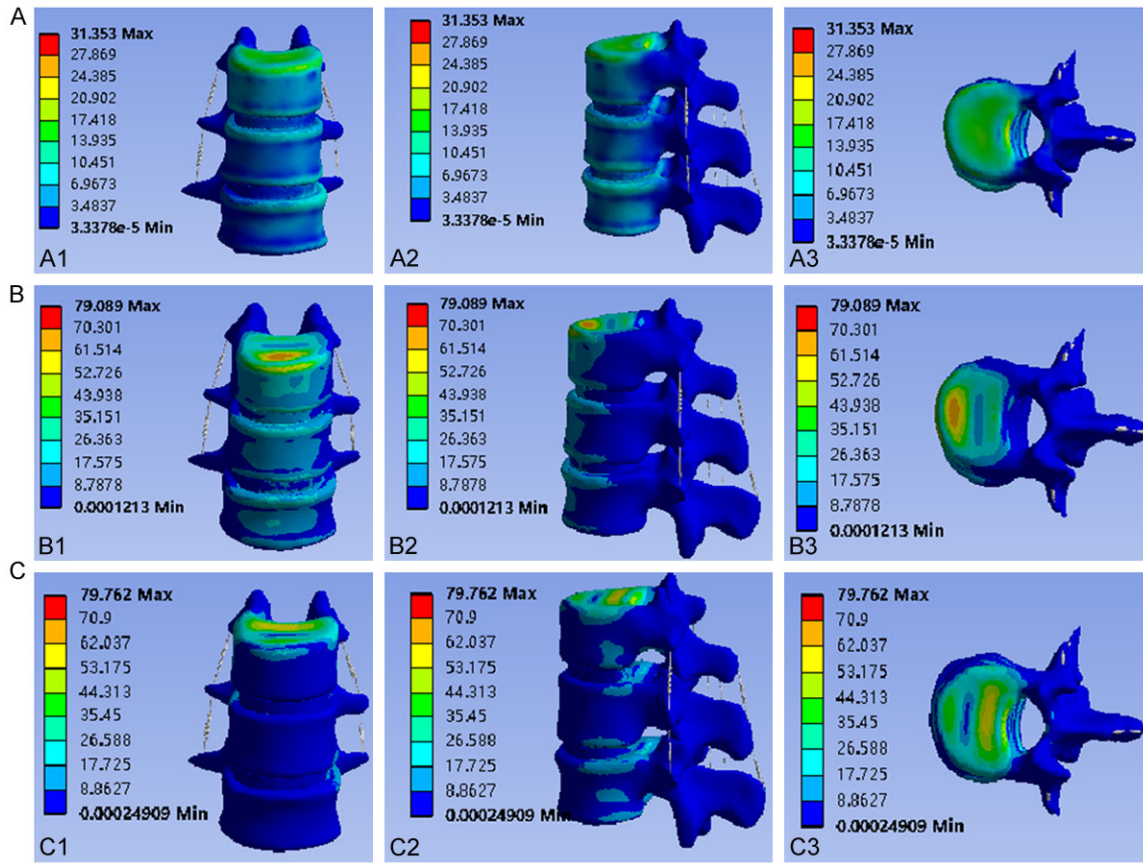


Figure 6. Three-view results of von-Mises stress distribution of T12-L2 finite element model in thoracic and lumbar segments in Axial Direction, Ante-flexion and Rear Protraction. (A1) Axial Direction-front view, (A2) Axial Direction-side view, (A3) Axial Direction-top view; (B1) Ante-flexion-front view, (B2) Ante-flexion-side view, (B3) Ante-flexion-top view; (C1) Rear Protraction-front view, (C2) Rear Protraction-side view, (C3) Rear Protraction-top view.

acted as an upright strut and significantly reduced the convexity of the reinforced endplate. The bulge of the thickened endplate was reduced to 7% of its pre-thickening level, and the whole motion segment hardened by approximately 11%.

Noailly et al. applied finite element analysis to study the effect of prosthetic replacement of the physiological L4-L5 intervertebral disc on biomechanical changes of the L3-L4 lumbar segmental model [19]. Biomechanical analysis was performed by substituting L4-L5 discs in the L3-L5 lumbar segmental physiological model to simulate the role of loads in physiological states of compression, bending, extension, and axial rotation. The disc replacement model was found to be more rigid than the physiological model. When placed in perfect contact with the adjacent vertebra, the implanted disc is able to function, following the

biomechanics of the surrounding motion segment. Although the trauma load within adjacent vertebrae was not calculated, bone remodeling was expected in the trabeculae. Using numerical methods, this study allows for prediction of the static mechanical behavior of new devices within the lumbar spine structure, which can be useful for clinical studies.

Characteristics in this research

The 3D finite element model of this experiment had the following characteristics: 1) CT data for the thoracolumbar T12-L2 segment were obtained from a 65-year-old female volunteer. ANSYS finite element software was used for analysis, each structure of the thoracic and lumbar T12-L2 segment was simulated, and the model was realistic. 2) Compared to biomechanical analysis of cadaver specimens, the finite element software used in this study was

Biomechanical analysis of the spine

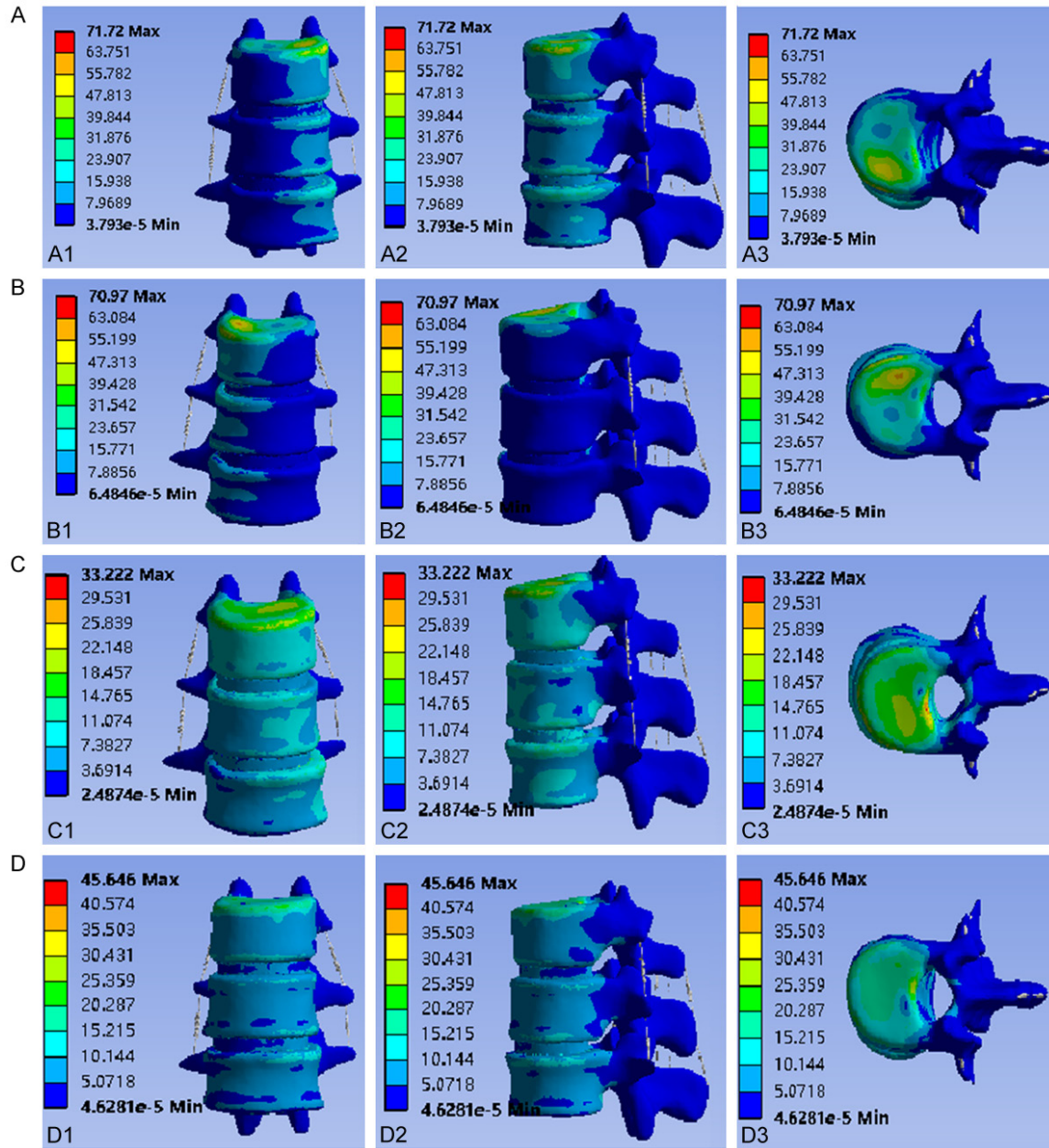


Figure 7. Results of von-Mises stress distribution of the T12-L2 finite element model in the thoracic and lumbar segments in three views under the states of Left Side Bending, Right Side Bending, Left Rotation and Right rotation. (A1) Left Side Bending-front view, (A2) Left Side Bending-side view, (A3) Left Side Bending-top view; (B1) Right Side Bending-front view, (B2) Right Side Bending -side view, (B3) Right Side Bending-top view; (C1) Left Rotation-front view, (C2) Left Rotation-side view, (C3) Left Rotation-top view; (D1) Right rotation-front view, (D2) Right rotation- side view, (D3) Right rotation-top view.

easy to operate and repeatable. 3) The model in this study adopted the method of assembly node sharing, and the complete model had 31,902 nodes and 64,244 cells. Without affecting experimental results, the number of grids was simplified and the calculation time was reduced. 4) Various conditions can be sim-

ulated in clinical practice by adjusting the material properties of each structure in the model.

Limitations in this research

This study, while robust, has some limitations. 1) The physiological activity states of only 7 ver-

tebral bodies were simulated, while a living human spine is larger and more complex. 2) Only finite element analysis software was tested, which limited comparisons with biomechanical test results of cadaver specimens. 3) Although the structure of each part of the thoracic and lumbar segment was accurately simulated with software, living human anatomy also contains skin, muscle, nerve, blood vessels, and other structures which cannot be simulated effectively.

Conclusions

Our experimental results provide a reference for clinical work and help to establish a three-dimensional finite element model of the thoracolumbar segment. In future studies, we aim to provide finite element analysis results that even more accurately represent normal and clinical cases.

Acknowledgements

This work was supported in part by Hubei Provincial Natural Science Foundation Committee General Project (2020CFB548) (Research and development of 3D printing rehabilitation AIDS design key technology based on topology optimization technology) and Science and Technology Support Plan Project of Guizhou Province in 2021 (2021584132938-20389) (Development and Industrialization of Adaptive Implant Devices for Bone Defect Regeneration in Children).

Disclosure of conflict of interest

None.

Address correspondence to: Dr. Qimei Wu, Wuhan Liu Sanwu Hospital of Traditional Chinese Medicine, Xinzhou District, Wuhan, Hubei, China. Tel: +86-17607245095; E-mail: 54211540@qq.com; Dr. Rong Liu, Department of Orthopedics, Puren Hospital Affiliated to Wuhan University of Science and Technology, 1 Benxi Road, Wuhan, Hubei, China. Tel: +86-15871811767; E-mail: dr_liurong@whu.edu.cn

References

[1] Daisuke N, Tsukasa K, Norihiro N, Saki I, Junji O, Hidenori S, Yasuaki I, Masahiro F, Xian C and Toshihiko T. Finite element analysis of compression fractures at the thoracolumbar junction

- using models constructed from medical images. *Exp Ther Med* 2018; 15: 3225-3230.
- [2] Crawford RP, Rosenberg WS and Keaveny TM. Quantitative computed tomography-based finite element models of the human lumbar vertebral body: effect of element size on stiffness, damage, and fracture strength predictions. *J Biomech Eng* 2003; 125: 434-438.
- [3] Crawford RP, Cann CE and Keaveny TM. Finite element models predict in vitro vertebral body compressive strength better than quantitative computed tomography. *Bone* 2003; 33: 744-750.
- [4] Belytschko T, Kulak RF, Schultz AB and Galante JO. Finite element stress analysis of an intervertebral disc. *J Biomech* 1974; 7: 277-285.
- [5] Xu H, Tang H, Guan X, Jiang F, Xu N, Ju W, Zhu X, Zhang X, Zhang Q and Li M. Biomechanical comparison of posterior lumbar interbody fusion and transforaminal lumbar interbody fusion by finite element analysis. *Neurosurgery* 2013; 72: 21-26.
- [6] Lo CC, Tsai KJ, Chen SH, Zhong ZC and Hung C. Biomechanical effect after Coflex and Coflex rivet implantation for segmental instability at surgical and adjacent segments: a finite element analysis. *Comput Methods Biomech Biomed Engin* 2011; 14: 969-978.
- [7] Chen SH, Lin SC, Tsai WC, Wang CW and Chao SH. Biomechanical comparison of unilateral and bilateral pedicle screws fixation for transforaminal lumbar interbody fusion after decompressive surgery—a finite element analysis. *BMC Musculoskelet Disord* 2012; 13: 72.
- [8] Goel VK and Gilbertson LG. Applications of the finite element method to thoracolumbar spinal research—past, present, and future. *Spine (Phila Pa 1976)* 1995; 20: 1719-1727.
- [9] Hsu CC, Chao CK, Wang JL, Hou SM, Tsai YT and Lin J. Increase of pullout strength of spinal pedicle screws with conical core: biomechanical tests and finite element analyses. *J Orthop Res* 2005; 23: 788-794.
- [10] Kiliñer C, Inceoglu S, Sohn MJ, Ferrara L and Benzel EC. Effects of angle and laminectomy on triangulated pedicle screws. *J Clin Neurosci* 2007; 14: 1186-1191.
- [11] Hashemi A, Bednar D and Ziada S. Pullout strength of pedicle screws augmented with particulate calcium phosphate: an experimental study. *Spine J* 2009; 9: 404-410.
- [12] Sairyo K, Goel VK, Masuda A, Vishnubhotla S, Faizan A, Biyani A, Ebraheim N, Yonekura D, Murakami RI and Terai T. Three-dimensional finite element analysis of the pediatric lumbar spine. Part I: pathomechanism of apophyseal bony ring fracture. *Eur Spine J* 2006; 15: 923-929.

Biomechanical analysis of the spine

- [13] Sairyo K, Goel VK, Masuda A, Vishnubhotla S, Faizan A, Biyani A, Ebraheim N, Yonekura D, Murakami RI and Terai T. Three dimensional finite element analysis of the pediatric lumbar spine. Part II: biomechanical change as the initiating factor for pediatric isthmic spondylolysis at the growth plate. *Eur Spine J* 2006; 15: 930-935.
- [14] Lee KK, Teo EC, Fuss FK, Vanneuville V, Qiu TX, Ng HW, Yang K and Sabitzer RJ. Finite-element analysis for lumbar interbody fusion under axial loading. *IEEE Trans Biomed Eng* 2004; 51: 393-400.
- [15] Schmidt H, Heuer F, Simon U, Kettler A, Rohlmann A, Claes L and Wilke HJ. Application of a new calibration method for a three-dimensional finite element model of a human lumbar annulus fibrosus. *Clin Biomech (Bristol, Avon)* 2006; 21: 337-344.
- [16] Rohlmann A, Boustani HN, Bergmann G and Zander T. A probabilistic finite element analysis of the stresses in the augmented vertebral body after vertebroplasty. *Eur Spine J* 2010; 19: 1585-1595.
- [17] Baroud G, Nemes J, Heini P and Steffen T. Load shift of the intervertebral disc after a vertebroplasty: a finite-element study. *Eur Spine J* 2003; 12: 421-426.
- [18] Goel VK, Kong W, Han JS, Weinstein JN and Gilbertson LG. A combined finite element and optimization investigation of lumbar spine mechanics with and without muscles. *Spine (Phila Pa 1976)* 1993; 18: 1531-1541.
- [19] Noailly J, Lacroix D and Planell JA. Finite element study of a novel intervertebral disc substitute. *Spine (Phila Pa 1976)* 2005; 30: 2257-2264.
- [20] Zhang L, Yang G, Wu L and Yu B. The biomechanical effects of osteoporosis vertebral augmentation with cancellous bone granules or bone cement on treated and adjacent non-treated vertebral bodies: a finite element evaluation. *Clin Biomech (Bristol, Avon)* 2010; 25: 166-172.
- [21] Liang D, Ye LQ, Jiang XB, Yang P, Zhou GQ, Yao ZS, Zhang SC and Yang ZD. Biomechanical effects of cement distribution in the fractured area on osteoporotic vertebral compression fractures: a three-dimensional finite element analysis. *J Surg Res* 2015; 195: 246-256.
- [22] Chung SK, Kim YE and Wang KC. Biomechanical effect of constraint in lumbar total disc replacement: a study with finite element analysis. *Spine (Phila Pa 1976)* 2009; 34: 1281-1286.
- [23] Liang D, Ye LQ, Jiang XB, Yang P, Zhou GQ, Yao ZS, Zhang SC and Yang ZD. Biomechanical effects of cement distribution in the fractured area on osteoporotic vertebral compression fractures: a three-dimensional finite element analysis. *J Surg Res* 2015; 195: 246-256.
- [24] Panjabi MM, Kifune M, Liu W, Arand M, Vasavada A and Oxland TR. Graded thoracolumbar spinal injuries: development of multidirectional instability. *Eur Spine J* 1998; 7: 332-329.
- [25] Yoganandan N, Myklebust JB, Ray G and Sances A Jr. Mathematical and finite element analysis of spine injuries. *Crit Rev Biomed Eng* 1987; 15: 29-93.
- [26] Yoganandan N, Kumaresan S, Voo L and Pintar FA. Finite element model of the human lower cervical spine: parametric analysis of the C4-C6 unit. *J Biomech Eng* 1997; 119: 87-92.
- [27] Zhu L, Wang J, Cao Y, Fan W, Yu G, Zhang X and Ye W. Finite element modeling of human lumbosacral vertebra based on CT data. *Chin J Tissue Engineering Research* 2012; 16: 5511-5515.
- [28] Liu Y, Tian Q, Li G, Yang S, Du J and Shao Z. A three-dimensional finite element model of lumbar spine with osteoporosis. *Journal of Lumbar Surgery* 2013; 30: 161-162.
- [29] Fu Y, Ruan D, Huo H, Yang X and Li C. A three-dimensional finite element model of lumbar spine based on CT scanning and CAD. *Chin J Tissue Engineering Research and Clinical Rehabilitation* 2011; 15: 1557-1561.
- [30] Huang J, Li H, Jian F and Yan H. A study of the effect of intervertebral disc herniation on intervertebral disc herniation. *Chin J Neuropathology* 2012; 12: 394-398.
- [31] Tang S and Meng X. Does disc space height of fused segment affect adjacent degeneration in ALIF? A finite element study. *Turk Neurosurg* 2011; 21: 296-303.
- [32] Yoganandan N, Kumaresan S, Voo L and Pintar FA. Finite element applications in human cervical spine modeling. *Spine (Phila Pa 1976)* 1996; 21: 1824-1834.
- [33] Yoganandan N, Kumaresan S and Pintar FA. Biomechanics of the cervical spine Part 2. Cervical spine soft tissue responses and biomechanical modeling. *Clin Biomech (Bristol, Avon)* 2001; 16: 1-27.
- [34] Giambini H, Qin X, Dragomir-Daescu D, An KN and Nassr A. Specimen-specific vertebral fracture modeling: a feasibility study using the extended finite element method. *Med Biol Eng Comput* 2016; 54: 583-593.